machines

Article

Online Monitoring of Surface Quality for Diagnostic Features in 3D Printing

Natalia Lishchenko [1], Ján Piteľ [1,*] and Vasily Larshin [2]

[1] Department of Industrial Engineering and Informatics, Faculty of Manufacturing Technologies, Technical University of Kosice, Bayerova 1, 080 01 Prešov, Slovakia; natalia.lishchenko@tuke.sk
[2] Department of Digital Technologies in Engineering, Odessa Polytechnic National University, 1 Shevchenko Ave., 65044 Odessa, Ukraine; vasilylarshin@gmail.com
* Correspondence: jan.pitel@tuke.sk; Tel.: +421-55602-6455

Abstract: Investigation into non-destructive testing and evaluation of 3D printing quality is relevant due to the lack of reliable methods for non-destructive testing of 3D printing defects, including testing of the surface quality of 3D printed parts. The article shows how it is possible to increase the efficiency of online monitoring of the quality of the 3D printing technological process through the use of an optical contactless high-performance measuring instrument. A comparative study of contact (R130 roughness tester) and non-contact (LJ-8020 laser profiler) methods for determining the height of irregularities on the surface of a steel reference specimen was performed. It was found that, in the range of operation of the contact method (Ra 0.03–6.3 µm and Rz 0.2–18.5 µm), the errors of the contactless method in determining the standard surface roughness indicators Ra and Rz were 23.7% and 1.6%, respectively. Similar comparative studies of contact and non-contact methods were performed with three defect-free samples made of plastic polylactic acid (PLA), with surface irregularities within the specified range of operation of the contact method. The corresponding errors increased and amounted to 65.96% and 76.32%. Finally, investigations were carried out using only the non-contact method for samples with different types of 3D printing defects. It was found that the following power spectral density (PSD) estimates can be used as diagnostic features for determining 3D printing defects: Variance and Median. These generalized estimates are the most sensitive to 3D printing defects and can be used as diagnostic features in online monitoring of object surface quality in 3D printing.

Keywords: signal processing; monitoring system; laser profiler; surface roughness; quality assessment; non-contact method; vision-based method; frequency analysis

check for updates

Citation: Lishchenko, N.; Piteľ, J.; Larshin, V. Online Monitoring of Surface Quality for Diagnostic Features in 3D Printing. *Machines* **2022**, *10*, 541. https://doi.org/10.3390/machines10070541

Academic Editor: César M. A. Vasques

Received: 28 May 2022
Accepted: 30 June 2022
Published: 4 July 2022

1. Introduction

The statistics show the growth in size of the global 3D printing market from 2013 to the present. For example, in 2020, the most popular use cases for 3D printing were prototyping (68%), proofs of concept (59%), production (49%) and R&D (42%) [1]. Nowadays, 3D printing is used in the aerospace, automotive, military, food, healthcare and medicine, architecture, fashion and electrical and electronics industries. The following materials can be used in 3D printing: metals, polymers and plastics, ceramics and composites [2].

Fused deposition modeling (FDM), associated with the Stratasys trademark, is currently the most widely used 3D printing technology. FDM printers use a thermoplastic filament, which is heated to its melting point and then extruded layer by layer to create a three-dimensional object. One of the key strengths of the FDM technique is its compatibility with various types of thermoplastic polymers. The most popular and stable materials are acrylonitrile butadiene styrene (ABS) and polylactic acid (PLA). FDM printers have demonstrated the ability to print other thermoplastics, which currently include polycarbonates (PCs), polystyrene (PS), polyamide, polyetherimide (PEI) and polyetheretherketone (PEEK).

There is also a demand for construction of composite filaments by adding certain materials into polymer matrices, as they can offer improved mechanical properties, biocompatibility, or conductivity [3–5].

To address the differences between additive manufacturing (AM) and conventional or subtractive manufacturing (SM), the science and engineering community is gravitating toward an AM solution centered on three pillars [6]:

1. Quality assurance (QA) derived from build planning (the use of advanced modeling and simulation to develop a plan for a machine to produce a specific part);
2. Build monitoring and inspection (monitoring the build process with sensors while the part is being constructed);
3. Feedback control to link the previous pillars together (using data from the build monitoring sensors to iteratively update the build plan).

In the right applications, additive manufacturing delivers a perfect trifecta of improved performance, complex geometries, and simplified fabrication [3].

Fundamentally, quality is about a part's ability to perform the task for which it has been designed while maintaining structural integrity. Contributing factors are usually included in a part's specifications and typically include geometry (the shape of the finished part and how it fits with other parts), surface finish (the desired smoothness, roughness, or other functional surface treatment of the finished part), and material properties (a variety of attributes, including mechanical strength, stiffness, and fatigue life) [6].

The advantages of the FDM method include easy handling, high printing speed, cost efficiency, the variety of types of thermoplastic polymers, the capacity for freeform fabrication without the use of expensive moulding sand tools, and the low cost of machines and consumables. The disadvantages of the FDM method include the different types of defects:

- Surface defects (over-extrusion [7], overheating [7], high roughness [8], stringy first layer [8]);
- Structure defects (cracking [9–12], under-extrusion [7,13,14], porosity [15,16]);
- Form defects (overheating [7], warping [9,10,17], blistering [9], stringing [9], layer shifting [18,19]).

Indirect and direct control methods can be used for the quality assessment of 3D printing. For indirect control, researchers have used acoustic emission (AE) signals [20–23], thermal cameras [24–26], vibration signals [27,28], current sensors [29,30], etc.I Indirect methods of quality control are most often used to detect different printing failures [20–31]; for example, those shown in Table 1, which indicates both the failures and signal (or sensor) types. These methods are indirectly related to the surface quality of printed 3D objects.

Table 1. Signals and sensors used for indirect monitoring [20–31].

Sensor (Signal) Type	Quality Characteristics
Accelerometer	Nozzle clogging Filament jamming Material leakage Extrusion stopping
Thermal camera	Nozzle clogging Irregular material flow
Acoustic emission	Filament breakage Extruder state Fan activity
Current, force, and pressure	Nozzle clogging Sabotage attacks in G-code Extrusion pressure Material flow rate

To implement direct methods quality control that can be embedded into the online surface quality monitoring system, a computer vision approach has become widespread. This is due to:

- The diverse methods available for assessing the quality of images;
- The possibility of using multiple cameras simultaneously to capture images from several sides of the printed object;
- The possibility of using advanced machine learning algorithms for image processing and quality assessment, such as support vector machines (SVMs), convolutional neural networks (CNNs), decision trees, etc. [32,33];
- The ease with which cameras can be integrated into equipment;
- The wide variety of image quality characteristics that can be evaluated with cameras (geometric deviations, infill structures, layer shifting, and surface defects, such as voids, overfill, underfill, blobs, cracks, misalignment, warping, detachment (delamination), etc.).

In computer vision systems, three main methods for assessing the quality of a manufactured object (that is, 3D printing system output parameters, which constitute a subjective classification as opposed to a scientific, statistical one and machine-learning algorithms) can be distinguished and used, namely:

1. Surface quality assessment; i.e., the presence of defects, such as voids, cracks, blobs, and misalignment;
2. Determination of geometric deviations in the dimensions of a printed object through comparison with the object's CAD model;
3. Determination of the print output parameters, such as layer, height, layer contour, material color, etc.

Among the disadvantages of this direction, researchers have noted the need to interrupt the printing process to capture an image, the large amount of data needed for training models, and the need for separate algorithms to identify different printing defects.

A review of the literature on the direct method for printed product quality assessment showed that most studies are devoted to the detection of surface defects that determine surface integrity. Therefore, this is an actual direction of quality control in additive manufacturing technologies. Since the FDM method is characterized by the periodicity of the pattern, the application of Fourier analysis is one possible direction that could be interesting, both here as well as in other applications, including for drilling [34] and milling [35]. For example, Fourier analysis has been used for no-reference estimation of 3D printed surface quality [36]. For this, two different fragments with "good" and "bad" quality are selected from the same sample. The image is converted into shades of gray (grayscale) and the spectrum is built from the original signal perpendicular to the layers of the filament. For high-quality printing, the regular pattern results in explicit peaks in the Fourier domain but, in the presence of structural distortion, there are no peaks. As the numerical value allowed the determination of the quality of the analyzed fragments of the samples, the authors used the integral of the spectra values calculated using the trapezoidal rule. High values for the specified parameter indicated low quality for the fragment and low values indicated high quality. The authors noted that the results for the integral were highly dependent on the color of the sample. It also became necessary to use different threshold values to distinguish between high and low quality samples. They analyzed images only in the frequency domain, ignoring the time domain, analysis of which can contribute, for example, to identifying various types of defects and distortions in the sample geometry, determining the layer thickness, etc.

Frequency analysis is considered to improve quality in Big Area Additive Manufacturing [37]. The authors of this study also noted the rationale for using Fourier analysis for horizontal stacked lines with a given periodicity in the y-direction. Fourier analysis provides insights into the layer thickness and its variation. The presence of a tall, thin spike at the dominant frequency means that the print is regular. An increase in peak width with a decrease in its amplitude indicates slumping of material and extrusion at an excessively high temperature. Further slumping leads to a more than twofold increase in the width of the peak in comparison to the reference peak. Thus, the image analysis in [36] was performed only in the frequency domain, and no quantitative indicator was proposed that could be used as a diagnostic indicator for the monitoring system.

Laser profilometry has recently been increasingly used for non-contact measurement of profile irregularities; e.g., surface roughness parameters (Figure 1a). The influence of both the material type and cutting speed on surface roughness using an abrasive water jet has been studied with a special measurement scheme [38], but more modern equipment was used for plastics in this study (Figure 1b).

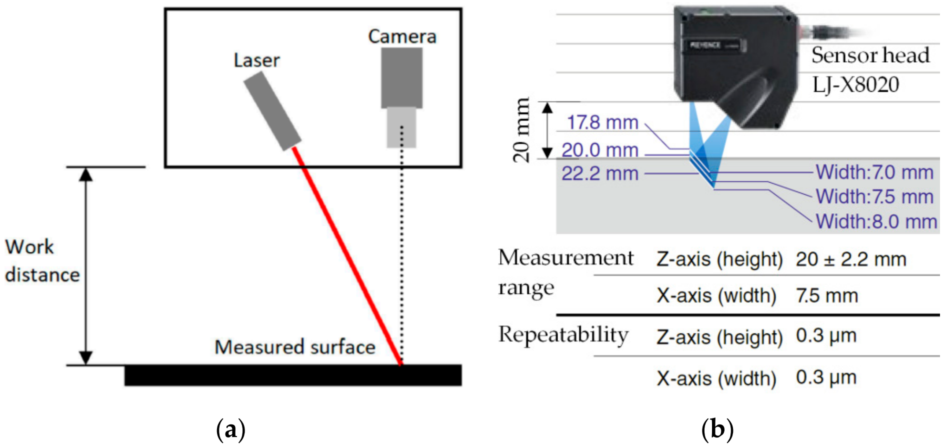

Figure 1. Measurement schemes using laser profilometry: (**a**) composite [38]; (**b**) integrated.

The surface roughness parameters of the metal samples were measured using both a laser profilometer (Contactless LPM, 2015, KVANT spol. s.r.o., Bratislava, Slovakia) and a conventional contact roughness meter (Mitutoyo SJ 400, Mitutoyo America Corporation, Aurora, FL, USA). It was found that the Ra values measured by the laser profilometer lay within the range of the values measured by the Mitutoyo SJ 400, while the obtained Rz values were two to three times lower than the values measured with the laser profilometer. The reasons were that noise occurred when measuring some areas of the surface with the laser profilometer due to the reflection of the complementary metal–oxide–semiconductor (CMOS) camera and because the measuring tip of the contact meter could not sense all the surface irregularities.

The LPM 4 laser profilometer was used for the unevenness measurement of the beech sample surface. When doing so, the reference material in the experiment was an aluminum standard with a surface roughness value Ra = 10 µm. The optical non-contact method is a much faster, more accurate, and more reliable solution compared to manual measurement systems. Furthermore, the optimal wavelength was identified experimentally and higher accuracy and sensitivity with the blue light were confirmed.

A constructed laser profiler has been presented and investigations were carried out to verify the developed device's accuracy through the comparison of the measured data with the standard [37]. It was noted that the value obtained for the Ra parameter with the laser profiler turned out to be higher than the standard value. The pros of the laser profiler were its measurement speed and acceptable price. Its cons were that the shape of the object to be measured had to not be too curved and the surface of the object had to not be glossy. The latter was because, when measuring glossy surfaces, a large amount of the laser light incident on the surface components was reflected back to the charge-coupled device (CCD) camera.

Thus, the review demonstrates that non-contact methods for surface quality control have advantages for 3D printing. Laser profilometry (2D measurement and 3D inspection) and vision-based methods are the most promising in this context. Laser profilers have been used to determine the absolute values of many surface profile parameters [39,40]. However, the influence of the reflectivity of the material to be used may introduce an error in the measurement results. However, the differentiated initial quality of the surface under study requires that certain settings be implemented on the laser profilometer to obtain the correct result. For these reasons, the numerical values of the profile parameters obtained using a laser profiler and a contact device may differ. This is why it is necessary to investigate this difference and establish appropriate links between the results from contact and non-contact measurements.

To develop mathematical software for an online quality monitoring system for 3D parts, it is necessary to create information signals containing the diagnostic signs that characterize the change in quality of the 3D part during 3D printing, and which can be used to monitor the state of the 3D printing system [41]. In addition, these diagnostic signs should provide information about the presence or absence of defects that may occur during the printing of plastic objects, as the roughness parameters do not provide such information. A possible reason for this is that the roughness parameters represent an integral assessment of the surface quality. This also needs to be investigated. In addition, given the periodic texture of the printed surface, it would be useful to investigate evaluation functions for online monitoring in the time and frequency domains using Fourier analysis.

Existing in situ monitoring techniques differ depending on the features of the laser additive manufacturing. For example, laser-induced breakdown spectroscopy (LIBS) has been suggested for in situ and real-time elemental analysis of cladding, as well as for cladding process failure detection [42]. In situ monitoring and ex situ elasticity mapping were introduced in [43], where an ultrasonic time-of-flight measurement monitoring technique was numerically and experimentally used to study the behavior of laser-induced melting pools. Furthermore, in situ X-ray imaging of defects has been deployed in laser additive manufacturing [44], as well as in situ thermal imaging for single-layer build-time alteration [45].

The aim of this research was therefore to develop information signals in the time and frequency domains that contain the surface quality diagnostic features (signs) for in situ monitoring of the 3D printing system state.

2. Materials and Methods

The test samples were made using the FDM method. A Creality Ender-3 3D printer, CREALITY, Shenzhen, China (Figure 2a) with a PLA filament was used for the research. The samples were designed with Autodesk Inventor Professional 2021 software. To generate the G-code for object printing, the conversion of the CAD model into the stereolithography (STL) format was undertaken with the Ultimaker Cura slicer software (a popular 3D printing software). The printing parameters were selected as shown in Table 2 [46].

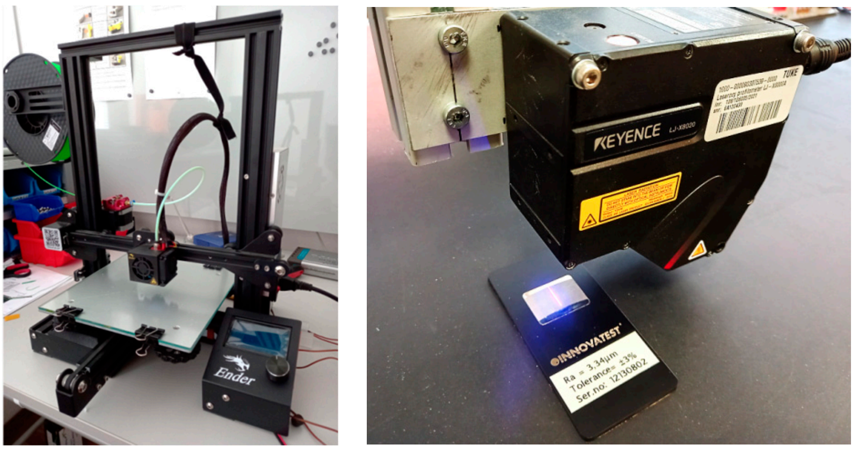

(**a**) (**b**)

Figure 2. (**a**) Creality Ender-3 3D printer; (**b**) LJ-8020 laser profiler with a metal sample.

Table 2. Printing process parameters.

Parameter	Value	Units
Nozzle diameter	0.4	mm
Filament size	1.75	mm
Layer thickness	0.2	mm
Raster angle	45.90	degree
Raster width	0.4	mm
Bed temperature	60	°C
Printing temperature	210	°C
Printing speed	45	mm/s
Infill density	20	%
Infill flow	100	%

A KEYENCE LJ-8020 laser profiler, KEYENCE INTERNATIONAL, Mechelen, Belgium (Figure 2b) was used to measure and evaluate the special samples (Figure 3) made of polylactic acid (PLA).

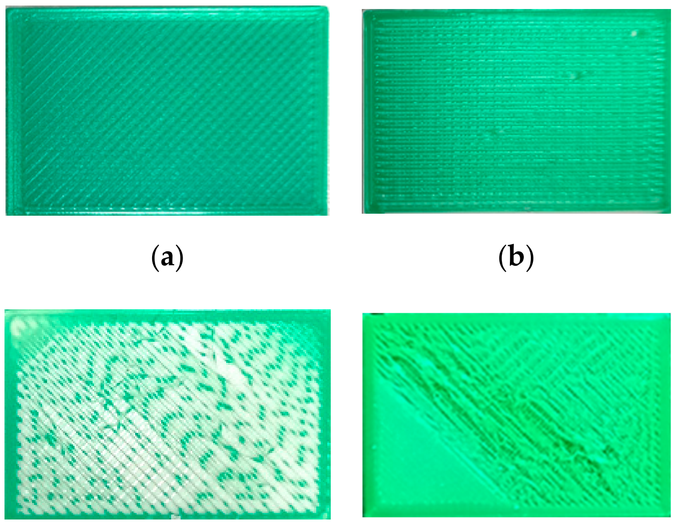

(**a**) (**b**) (**c**) (**d**)

Figure 3. Samples under investigation: (**a**) reference; (**b**) under-extrusion; (**c**) stringy first layer; (**d**) high roughness.

First, for verification, the surface roughness parameters of the metal specimen (Figure 4a) were determined using an R130 roughness tester (Figure 4b) and the LJ-8020 laser profiler (Figure 2b).

(**a**) (**b**)

Figure 4. (**a**) Specimen measured to determine roughness parameters; (**b**) R130 roughness tester at work.

Several defect-free 3D printed samples (Figure 5) were simultaneously measured and evaluated with the Innovatest R130 roughness tester (INNOVATEST Europe BV, Maastricht, The Netherlands) and the KEYENCE LJ-8020 laser profiler (Figure 6a) to compare the results obtained using contact and contactless instruments, respectively.

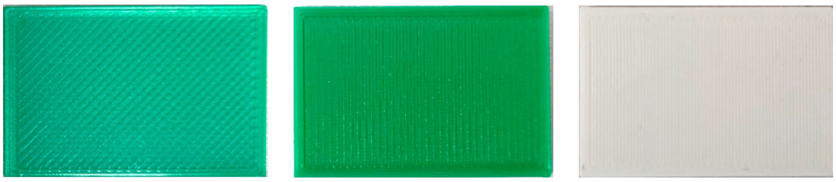

(**a**) (**b**) (**c**)

Figure 5. Defect-free samples for study: (**a**) green sample with +45° raster angle; (**b**) green sample with 90° raster angle; (**c**) white sample with 90° raster angle.

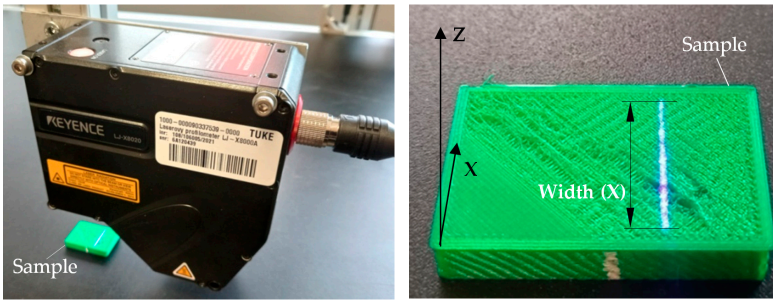

(**a**) (**b**)

Figure 6. Setup for measuring a plastic object: (**a**) laser profiler with a sample; (**b**) defective green 3D sample (30 × 20 × 5 mm) under study.

The following KEYENCE equipment was used for the profile analysis: an LJ-8020 laser profiler (see Table 3 for specifications) and, as a separate unit, an LJ -X8000A controller (KEYENCE INTERNATIONAL, Mechelen, Belgium). The equipment was connected to LJ-X Navigator and LJ-X Observer software (KEYENCE CORPORATION OF AMERICA, Itasca, IL, USA) to show the profile parameters obtained by the laser profiler. Further, MS Excel, MatLAB, and NI-LabVIEW software were used for processing and presentation of measurement results.

Table 3. LJ-X8020 sensor head specifications.

Specification	Name	Value
Reference distance	*z*-axis (height)	20 mm
Measurement range	*x*-axis (width), near side *x*-axis (width), reference distance *x*-axis (width), far side	7 mm 7.5 mm 8 mm
Light source	Blue semiconductor Laser wavelength Class 2M laser product (IEC60825-1, FDA (CDRH) Part 1040.10) Output	405 nm (visible light) 10 mW
Spot size		Approx. 16 mm × 32 µm
Repeatability	*z*-axis (height) *x*-axis (width)	0.3 µm 0.3 µm
Profile data interval	*x*-axis (width)	2.5 µm
Profile data count		3200 points

3. Results and Discussion

3.1. Calibration of R130 Roughness Tester

The Innovatest R130 roughness tester had the following specifications:

- Ra and Rz measurement ranges: 0.03 μm–6.3 μm and 0.2 μm–18.5 μm, respectively;
- Display resolution: 0.01 μm;
- Cut-off: 0.25 mm; 0.8 mm; 2.5 mm;
- ANSI 2RC filter, Sino Age Development Technology, Ltd., Beijing, China.

Prior to operation, the R130 must be calibrated and checked using the reference specimen (Figure 4a). Calibration settings: cut-off—0.8 mm, traverse length—4.5 mm, evaluation length—4.0 mm, number of cut-offs—5. The results were as follows: Ra (1) = 3.24 μm, Ra (2) = 3.23 μm, and Ra (3) = 3.28 μm; i.e., the average mean Ra (ave) = 3.25 μm. According to the manual, if the reading is within ± 0.1 μm (3.24 μm < Ra < 3.34 μm), calibration is within tolerance. In our case, Ra (ave) = 3.25 μm was within the specified range. The Rz values (the maximum roughness depth or the largest of the peak-to-valley roughness depths across the evaluation length) were Rz (1) = 12.1 μm, Rz (2) = 12.3 μm, and Rz (3) = 12.1 μm; i.e., the average mean Rz (ave) = 12.17 μm (Table 4).

Table 4. Roughness parameters obtained for the metal reference specimen with the R130 roughness tester and LJ-8020 laser profiler.

Roughness Parameter	R130 Roughness Tester	LJ-X8020 Laser Profiler
Ra, μm	3.24 3.23 3.28 Average **3.25**	2.684 2.377 2.383 Average **2.481**
Rz, μm	12.1 12.3 12.1 Average **12.17**	12.740 11.554 12.800 Average **12.365**

Note: evaluation length: 4 mm.

Differences in μm and percentages for Ra and Rz between the measurements with LJ-8020 laser profiler and R130 tester are shown in Table 5.

Table 5. Average surface roughness parameters obtained for the metal reference specimen with the R130 roughness tester and LJ-8020 laser profiler.

Instrument and Error	Ra, μm	Rz, μm
LJ-X8020 laser profiler	2.481	12.365
R130 roughness tester	3.250	12.170
Difference, %	23.66	1.60

3.2. Roughness Parameter Measurement on the Metal Reference Specimen with Contact and Non-Contact Methods

The laser profiler (Figure 6a) uses a laser displacement sensor that collects height data across a laser line rather than a single point. This enables 2D/3D measurements, such as height difference, width, or angle, to be obtained using a single sensor; i.e., "three-in-one" measurements. A laser line is emitted from the sensor to illuminate the surface of a target. The reflected light is imaged by the complementary metal–oxide–semiconductor (CMOS) image sensor to create a profile of the surface, which can then be used for measurement and inspection.

The triangulation principle is used for measurement in the following sequence: (1) the laser beam is directed at the sample to be inspected, and then (2) the light reflected by the sample is collected by the receiver lens and (3) reproduced on the light-receiving element. When the distance changes, the collected light is reflected at a different angle, and the position of the beam on the light-receiving element changes accordingly.

To verify and compare the measured values, measurement of the metal specimen (Figure 4a) was also carried out using the R130 contact roughness tester (Table 4). The same part of the surface was selected for each sample with both methods of measurement; i.e., with the R130 contact roughness tester and the LJ-X8020 non-contact laser profiler.

When determining the roughness parameters using the laser profiler, the profile data interval was 2.5 µm and the profile data count was 3200 points; thus, the evaluation length in this case was 8 mm (2.5 µm × 3200 points = 8000 µm; i.e., 8 mm). When determining the roughness parameters using the R130, the evaluation length was 4 mm. Thus, the roughness parameters Ra and Rz, when evaluated using the laser profiler, were determined on two evaluation length segments of 4 mm each (Figure 7).

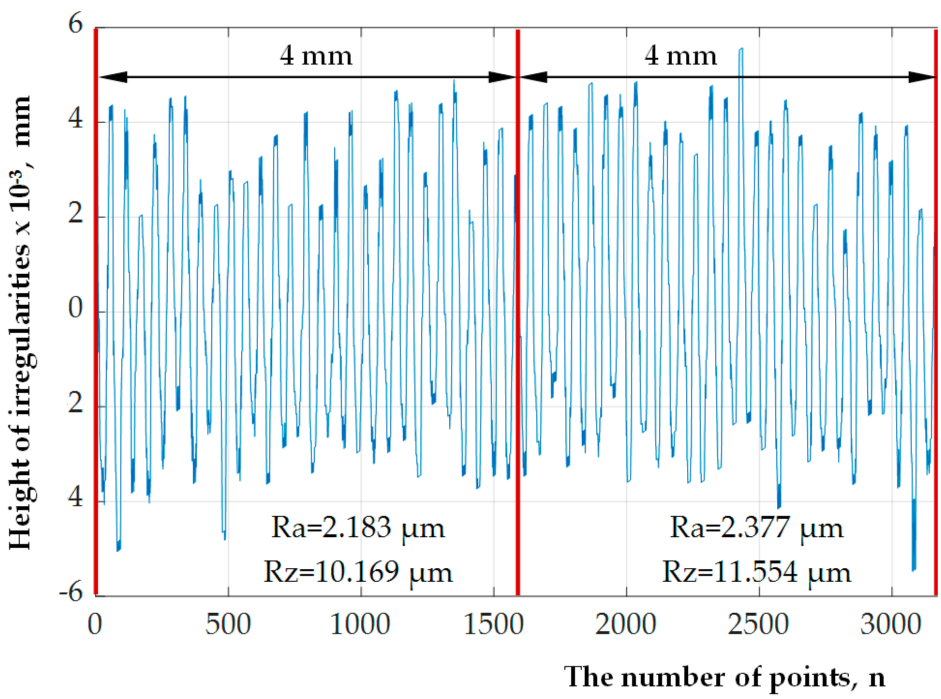

Figure 7. Surface roughness profile for metal specimen as measured by the LJ-8020 laser profiler.

Therefore, the roughness parameters obtained for the metal surface of the reference specimen (with 4 mm evaluation length) using contact (R130 roughness tester) and non-contact (LJ-8020 laser profiler) devices were close: Ra = 3.250 µm and Ra = 2.481 µm, and Rz = 12.170 µm and Rz = 12.365 µm.

3.3. Roughness Parameter Measurement for the Plastic Samples with Contact and Non-Contact Methods

To verify and compare the measured values, measurement of the samples shown in Figure 5 was carried out with both the contact R130 roughness tester (Table 6) and the LJ-8020 laser profiler (Table 7). The same part of the surface was selected for each sample with both methods of measurement. Table 6 shows the surface roughness response obtained with the R130 tester, along with the mean, for three FDM 3D printed parts.

Table 6. Plastic surface roughness parameters obtained with the R130 roughness tester.

Sample	Ra, µm	Rz, µm	Ra (Ave), µm	Rz (Ave), µm
Figure 5a	5.06 4.27 4.20	24.9 22.3 21.2	4.51	22.8
Figure 5b	9.22 8.97 9.32	25.0 25.0 25.0	9.17	25.0
Figure 5c	6.62 6.54 6.18	24.9 24.9 24.9	6.45	24.9

Note: cut-off: 2.5 mm; evaluation length: 2.5 mm; number of cut-offs: 1; Ra (ave) and Rz (ave) means are the averages of three measurements.

Table 7. Plastic surface roughness parameters obtained with the LJ-8020 laser profiler.

Sample	Ra, µm	Rz, µm	Ra (Ave), µm Difference	Rz (Ave), µm Difference
Figure 5a	9.155 8.219 6.984	39.903 41.496 33.211	8.119 **80.02%**	38.203 **67.56%**
Figure 5b	8.855 10.655 9.859	68.500 36.500 27.200	9.790 **6.79%**	44.060 **76.24%**
Figure 5c	14.325 14.135 12.381	57.233 30.464 50.626	13.614 **111.07%**	46.108 **85.17%**
Average difference			**65.96%**	**76.32%**

Note: evaluation length: 2.5 mm.

Table 7 shows the surface roughness response obtained with the LJ-8020 laser profiler, along with the mean, for three FDM 3D printed parts. The table also shows differences in percentages compared to the measurements with the R130 tester (Table 6). For example, when Ra (ave) = 4.51 µm (Table 6) and Ra (ave) = 8.119 µm (Table 7), the difference was 80.02%, because $\frac{|4.51-8.119|}{4.51}100\% = 80.02\%$.

Thus, the transition to another material (from metal to plastic) was accompanied by an increase in the difference between the contact and non-contact measurement results from 23.66% (Table 5) to 65.96% (Table 7)—i.e., 2.8 times—for Ra (ave) and from 1.6% (Table 5) to 76.32% (Table 7)—i.e., 47.7 times—for Rz (ave).

3.4. Diagnostic Feature Detection Using NI-LabVIEW

Modern computer measurement systems allow for the synthesis of new information signals in real time, which results from the mathematical processing of an array of primary digital data. For example, the NI-DAQmx measurement data acquisition system provided with the NI-LabVIEW software package has options for configuring information signals from the primary time signals of sensors. These options can be selected in the **Functions** menu using the **Functions**→**Express**→**Signal Analysis** scheme.

Two blocks are used in the **Signal Analysis** category:

1. The **Configure Statistics [Statistics]** block, which includes Range in the time domain and Arithmetic Mean, RMS, Standard Deviation, Variation, Median, Mode, and Summation in the frequency domain.
2. The **Configure Spectral Measurements** block, which includes the signal spectral characteristics Magnitude Peak, Power Spectrum, and Power Spectral Density (PSD) in the frequency domain.

For a comparative assessment of the informativeness of the newly generated signals when solving the problem of detecting defects on the surface of a printed sample in the NI-DAQmax computer data acquisition system provided with the NI-LabVIEW software package, information signals in the time domain (Range) and the frequency domain (Arithmetic Mean, RMS, Standard Deviation, Variation, Median, Mode, Summation) were studied. Using these signal processing tools, a Fourier analysis of the profilograms obtained using the laser profiler for the (**a**) reference, (**b**) under-extrusion, (**c**) stringy first layer, and (**d**) high roughness PLA plastic samples (Figure 3) was performed.

In the NI-LabVIEW software environment, the profilogram output signal (Figure 8) was fed to the **Configure Spectral Measurements** unit of the NI-LabVIEW system, which performs the fast Fourier transform (FFT) procedure. Of the three spectral characteristics of the **Configure Spectral Measurements** block (Magnitude Peak, Power Spectrum, and Power Spectral Density), the most sensitive spectral characteristic, Power Spectral Density (PSD), was used.

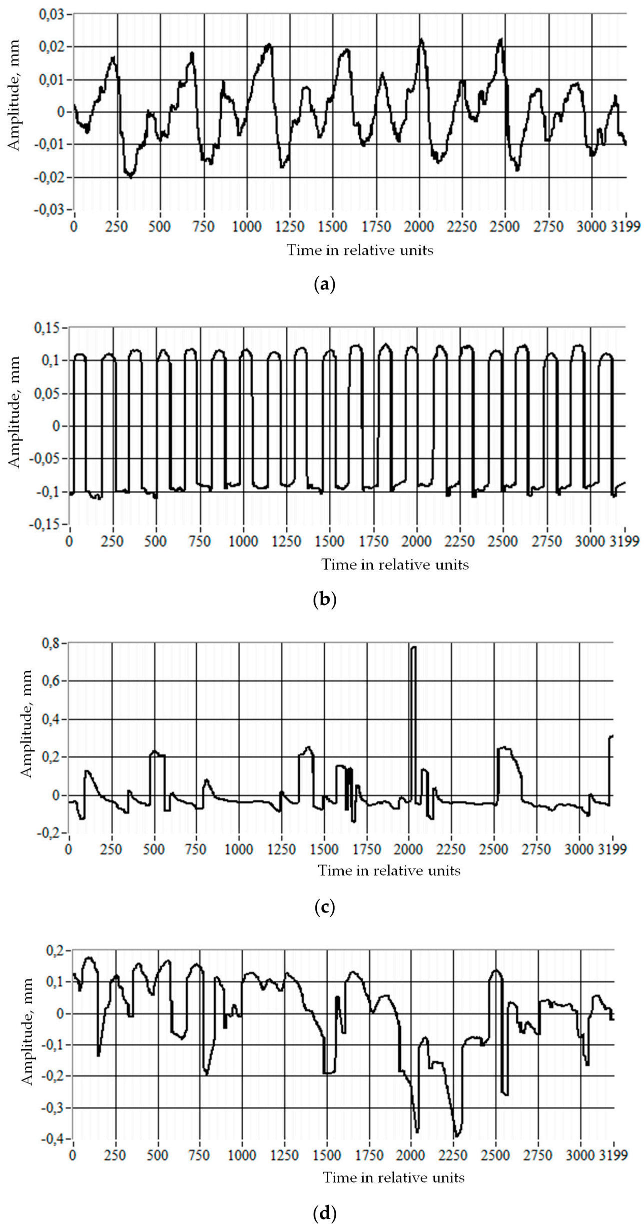

Figure 8. Initial profilograms in the time domain for four samples: (**a**) defect-free reference; (**b**) under-extrusion; (**c**) string first layer; (**d**) high roughness.

The results obtained after the FFT of the PSD configuration as displayed on the front panel of the virtual instrument of the NI-DAQmx system using **Waveform Graph** display units are shown in Figure 9.

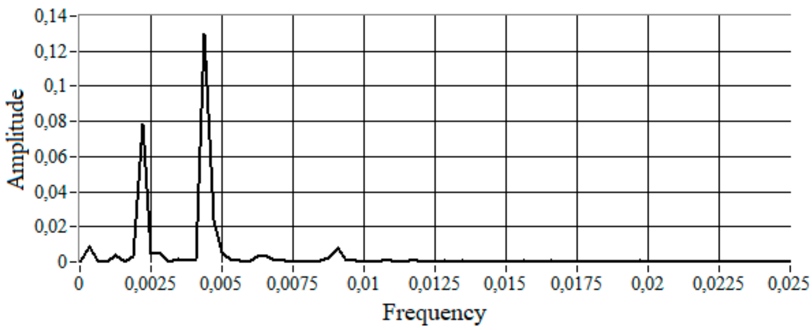

(**a**)

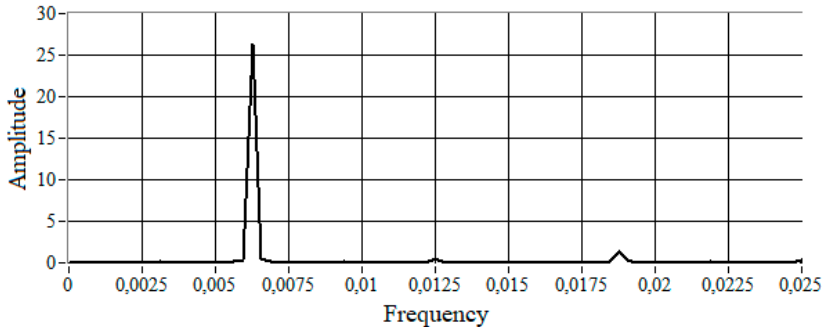

(**b**)

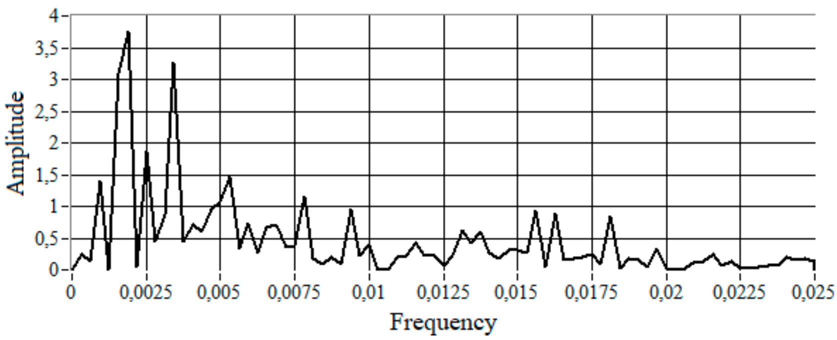

(**c**)

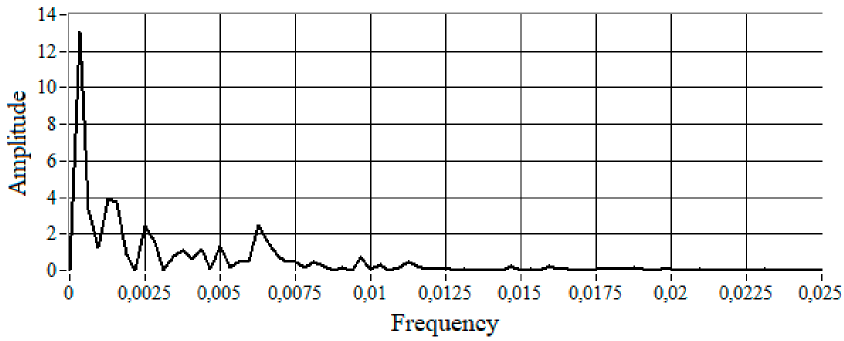

(**d**)

Figure 9. PSD spectra in the frequency domain: (**a**) reference sample; (**b**) under-extrusion; (**c**) stringy first layer; (**d**) high roughness.

Analyzing the PSD configuration data in Figure 9, the following intermediate conclusions can be formulated:

1. The PSD for a reference (defect-free) sample (Figure 9a) was characterized by four pronounced harmonics at the following relative frequencies (signal amplitudes are indicated in parentheses):
   - f1 = 0.000313 (A = 0,00885618);
   - f2 = 7f1 = 0.002188 (A = 0.0781748);
   - f3 = 14f1 = 0.004375 (A = 0.129859);
   - f4 = 28f1 = 0.009062 (A = 0.00748143).
2. The PSD for an under-extrusion-type defect sample (Figure 9b) was characterized by three harmonics at the following frequencies:
   - $f1^{/}$ = 20f1 = 0.00625 (A = 26.376);
   - $f2^{/}$ = 40f1 = $2f1^{/}$ = 0.0125 (A = 0.577246);
   - $f3^{/}$ = 60f1 = $3f1^{/}$ = 0.01875 (A = 1.41452).
3. The PSD for samples with stringy first layer (Figure 9c) and high roughness (Figure 9d) defects were characterized by a significant set of harmonics (with less pronounced amplitudes).

To quantify the PSD signal, the numerical values for the **Arithmetic Mean**, **RMS**, **Standard Deviation**, **Variance**, **Median**, **Mode**, and **Summation** parameters were determined after repetition of the same types of measurements three times, and then the averaged values of the corresponding signals were calculated (Table 8).

Table 8. Diagnostic feature values.

Diagnostic Sign	The Range- and PSD Signal-Averaged Values for the Plastic Samples in Figure 3			
	Reference	Under-Extrusion	Stringy First Layer	High Roughness
1 Range	0.04342(1)	0.25914(5.97)	0.65727(15.14)	0.92944(21.41)
2 Arithmetic Mean	0.00021(1)	0.02239(106.62)	0.03090(147.14)	0.04158(198.00)
3 RMS	0.00428(1)	0.69723(162.90)	0.36880(86.17)	0.36570(85.44)
4 Standard Deviation	0.00428(1)	0.69709(162.87)	0.36768(85.91)	0.36344(84.92)
5 **Variance**	1.844×10^{-5}(1)	0.48677(**26,397.5**)	0.13720(**7440.34**)	0.14937(**8100.32**)
6 **Median**	3.434×10^{-7}(1)	0.00030(**873**)	0.00020(**582**)	0.00049(**1426**)
7 Mode	0.00066(1)	0.13911(210.77)	0.05692(86.24)	0.04511(68.35)
8 Summation	0.33638(1)	35.8179(106.48)	49.4540(147.02)	66.5230(197.76)
Sum of ratings	8	28.03×10^3	8.60×10^3	10.20×10^3

Note: The numbers in brackets show the ratio of the indicator under consideration (one of three) to the indicator of the same name for the reference sample, taken as a unit.

3.5. Discussion

At the first stage, a comparative analysis of the results of contact (R130 roughness tester) and non-contact (LJ-8020 laser profiler) methods when measuring the same surface irregularities of a metal reference specimen with a known surface roughness was performed. The relative errors of the non-contact method in comparison to the contact method were established. The roughness parameters obtained for the metal surface of the reference specimen (with 4 mm evaluation length) using the contact (R130 roughness tester) and non-contact (LJ-8020 laser profiler) devices were close: Ra = 3.250 µm and Ra = 2.481 µm, and Rz = 12.170 µm and Rz = 12.365 µm. Thus, the contact and non-contact methods for control of standard integral parameters of surface roughness gave similar results for the metal reference specimen. The Errors in the parameters Ra and Rz in the range of operation of the R130 roughness tester were, respectively, 23.7 and 1.6%.

At the second stage, similar investigations were carried out with the plastic polylactic acid (PLA) samples in the range of operation of the contact method. The relative errors increased by 3 and 47 times, respectively, when determining the roughness parameters Ra and Rz. Thus, similar investigations with plastic parts were accompanied by much larger errors for the non-contact optical method (LJ-8020 laser profiler) compared to the contact method (R130 roughness tester): 65.96% and 76.32%, respectively, for the Ra and Rz integral roughness indicators.

At the third stage, diagnostic features were detected for online monitoring of three types of 3D printing defects—under-extrusion, stringy first layer, and high roughness—to produce diagnostic signs of 3D printing defects with the non-contact optical method (LJ-8020 laser profiler). The profilograms of the surfaces of the plastic parts were obtained, with each such profilogram being an analog representation of the change in the corresponding information signal over time. Next, the Fourier transforms of these information signals (i.e., the profilograms) were calculated and secondary information signals obtained. Integral estimates of PSD spectrograms can be produced in terms of the Arithmetic Mean, RMS, Standard Deviation, Variance, Median, Mode, and Summation.

Usually, the quality of 3D printed parts is checked after the completion of printing. As a result of our research, a system for monitoring the surface quality of the nth layer of a printed object in order to detect surface defects during printing can be proposed. The sampling step for 3D printing quality control can take place during the formation of one or more of the layers (Figure 10). In the block diagram below, the term "sign" is used instead of "feature" to highlight the difference between the productive (resulting) and methodological parts of the work.

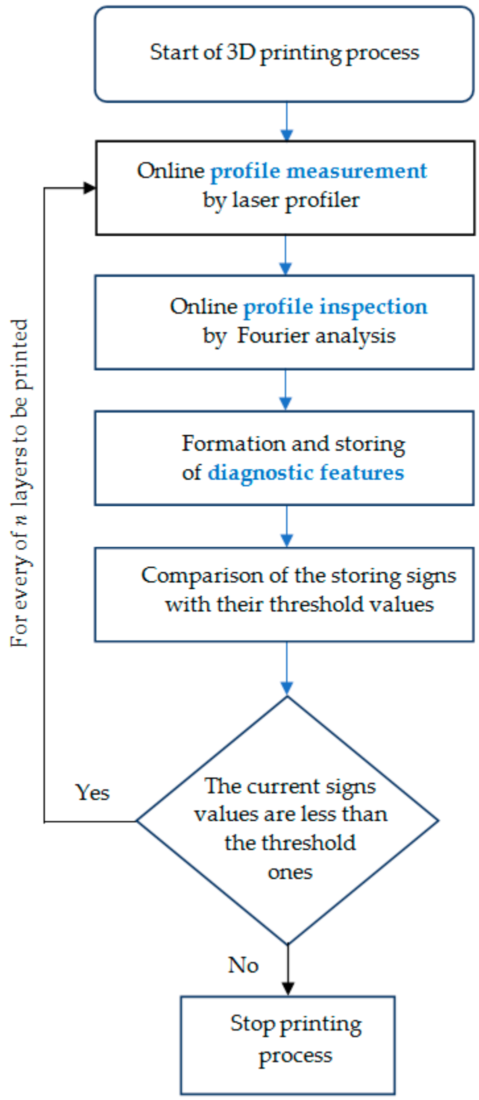

Figure 10. Monitoring algorithm block diagram.

4. Conclusions

The article proposed a new approach for online monitoring of object surface quality in 3D printing, especially for in situ monitoring. This monitoring is important in online printing quality control to prevent poor quality printing. A non-contact high-performance method was used to assess the irregularities on the surface of the part being manufactured. To confirm the feasibility of such an approach, comparative studies of contact (R130 roughness tester) and non-contact (LJ-8020 laser profiler) methods for assessing surface quality were carried out. It was established that the difference in the results of the quality assessment (with contact and non-contact methods) increased when moving from a metal sample to a plastic sample. For example, the transition from metal to plastic was accompanied by an increase in the difference between the measurement results of the contact and non-contact methods from 23.70% to 65.96% (2.8 times) and 1.6% to 76.32% (47.7 times), respectively, for Ra (ave) and Rz (ave).

When monitoring the 3D printing process of plastic parts online, in order to assess the quality of the process and the results of the 3D printing, the following (most defect-sensitive) integral estimates of PSD spectrograms can be used as diagnostic features of printing defects: Variance and Median. For example, the sensitivity of the integral estimate of Variance to defects such as under-extrusion, a stringy first layer, and high roughness was 26,397.50, 7440.34, and 8100.32, respectively. The least sensitive was the Range integral estimate in the initial surface profilogram of the plastic part (an information signal not subjected to the Fourier transform). For this Range estimate, the sensitivity to the previously listed three defects was 5.97, 15.14, and 21.41; i.e., significantly less.

The primary and secondary information signals generated by the non-contact method, as well as the methods for their formation, can be used when processing the topography of 3D printed object surfaces; i.e., when processing images of these surfaces in the online monitoring of 3D printed objects. Using these facts, further research can use the outlined monitoring strategy as a guide.

Author Contributions: Conceptualization, N.L. and V.L.; methodology, N.L. and J.P.; software, N.L.; validation, J.P. and V.L.; formal analysis, V.L.; investigation, N.L. and J.P.; resources, N.L. and J.P.; data curation, N.L.; writing—original draft preparation, N.L.; writing—review and editing, J.P.; visualization, N.L. and V.L.; supervision, V.L.; project administration, J.P.; funding acquisition, J.P. All authors have read and agreed to the published version of the manuscript.

Funding: This work was supported by the Slovak Research and Development Agency under the contract no. APVV-19-0590 and by the Ministry of Education, Science, Research and Sport of the Slovak Republic projects VEGA 1/0700/20 and 055TUKE-4/2020.

Institutional Review Board Statement: Not applicable.

Informed Consent Statement: Not applicable.

Data Availability Statement: The data presented in this study are available on request from the corresponding author.

Conflicts of Interest: The authors declare no conflict of interest.

References

1. Business Data Platform. Available online: https://www.statista.com (accessed on 22 February 2022).
2. Shahrubudin, N.; Lee, T.C.; Ramlan, R. An overview on 3D printing technology: Technological, materials, and applications. *Procedia Manuf.* **2019**, *35*, 1286–1296. [CrossRef]
3. Rahim, T.; Abdullah, A.; Akil, H. Recent developments in fused deposition modeling-based 3D printing of polymer sand their composites. *Polym. Rev.* **2019**, *59*, 589–624. [CrossRef]
4. Kaščak, J.; Gašpár, Š.; Paško, J.; Husár, J.; Knapčíková, L. Polylactic acid and its cellulose based composite as a significant tool for the production of optimized models modified for additive manufacturing. *Sustainability* **2021**, *13*, 1256. [CrossRef]
5. Kaščak, J.; Gašpár, Š.; Paško, J.; Knapčíková, L.; Husár, J.; Baron, P.; Török, J. Design of an atypical construction of equipment for additive manufacturing with a conceptual solution of a printhead intended for the use of recycled plastic materials. *Appl. Sci.* **2021**, *11*, 2928. [CrossRef]

6. Wing, I.; Gorham, R.; Sniderman, B. 3D Opportunity for Quality Assurance and Parts Qualification. Additive Manufacturing Clears the Bar. Available online: https://www2.deloitte.com/content/dam/insights/us/articles/3d-printing-quality-assurance-in-manufacturing/DUP_1410-3D-opportunity-QA_MASTER1.pdf (accessed on 28 February 2022).
7. 44 Issues Explained You're Your Prints Looking Perfect, Not Pathetic. Available online: https://rigid.ink/pages/ultimate-troubleshooting-guide (accessed on 13 March 2022).
8. First Layer Problems. Available online: https://3dprintguides.com/2020/04/3d-printing-first-layer-problems/ (accessed on 22 November 2021).
9. The Definitive Guide to Solving 3D Printing Problems by Bitlab. Available online: https://bitfab.io/blog/3d-printing-problems/ (accessed on 12 March 2022).
10. Fu, Y.; Downey, A.; Yuan, L.; Pratt, A.; Balogun, Y. In situ monitoring for fused filament fabrication process: A review. *Addit. Manuf.* **2021**, *38*, 101749. [CrossRef]
11. Okarma, K.; Fastowicz, J. Improved quality assessment of colour surfaces for additive manufacturing based on image entropy. *Pattern Anal. Appl.* **2020**, *23*, 1035–1047. [CrossRef]
12. Fastowicz, J.; Grudziński, M.; Tecław, M.; Okarma, K. Objective 3D printed surface quality assessment based on entropy of depth maps. *Entropy* **2019**, *21*, 97. [CrossRef] [PubMed]
13. Carlota, V. How to Avoid 3D Printing Problems. Available online: https://www.3dnatives.com/en/how-to-avoid-3d-printing-problems-26102020/ (accessed on 18 March 2022).
14. Jin, Z.; Zhang, Z.; Gu, G.X. Autonomous in-situ correction off used deposition modeling printers using computer vision and deep learning. *Manuf. Lett.* **2019**, *22*, 11–15. [CrossRef]
15. Kadam, V.; Kumar, S.; Bongale, A.; Wazarkar, S.; Kamat, P.; Patil, S. Enhancing surface fault detection using machine learning for 3D printed products. *Appl. Syst. Innov.* **2021**, *4*, 34. [CrossRef]
16. Wang, Y.; Huang, J.; Wang, Y.; Feng, S.; Peng, T.; Yang, H.; Zou, J. A CNN-based adaptive surface monitoring system for fused deposition modeling. *IEEE/ASME Trans. Mechatron.* **2020**, *25*, 2287–2296. [CrossRef]
17. 3D Printing First Layer Problems: Troubleshooting and How to Fix. Available online: https://www.elegoo.com/blogs/learn/3d-printing-first-layer-problems-troubleshooting-and-how-to-fix (accessed on 10 August 2021).
18. 3D Printer Layer Shifting. Available online: https://all3dp.com/2/layer-shifting-3d-printing-tips-tricks-to-solve-it/ (accessed on 23 May 2021).
19. Günaydin, K.; Türkmen, H.S. Common FDM 3D Printing Defects. In Proceedings of the 3rd International Congress on 3D Printing (Additive Manufacturing) Technologies and Digital Industry 2018, Antalya, Turkey, 19–21 April 2018; pp. 368–369.
20. Liu, J.; Hu, Y.; Wu, B.; Wang, Y. An improved fault diagnosis approach for FDM process with acoustic emission. *J. Manuf. Processes* **2018**, *35*, 570–579. [CrossRef]
21. Wu, H.; Wang, Y.; Yu, Z. In situ monitoring of FDM machine condition via acoustic emission. *Int. J. Adv. Manuf. Technol.* **2016**, *84*, 1483–1495. [CrossRef]
22. Wu, H.; Yu, Z.; Wang, Y. Real-time FDM machine condition monitoring and diagnosis based on acoustic emission and hidden semi-Markov model. *Int. J. Adv. Manuf. Technol.* **2017**, *90*, 2027–2036. [CrossRef]
23. Li, F.; Yu, Z.; Yang, Z.; Shen, X. Real-time distortion monitoring during fused deposition modeling via acoustic emission. *Struct. Health Monit.* **2019**, *19*, 412–423. [CrossRef]
24. Kousiatza, C.; Chatzidai, N.; Karalekas, D. Temperature Mapping of 3D Printed Polymer Plates: Experimental and Numerical Study. *Sensors* **2017**, *17*, 456. [CrossRef] [PubMed]
25. Dinwiddie, R.B.; Love, L.; Rowe, J.C.; Stockton, G.R.; Colbert, F.P. Real-time process monitoring and temperature mapping of a 3D polymer printing process. *Proc. SPIE* **2013**, *8705*, 87050L-1–87050L-9.
26. Ketai, H.; Huan, W.; Huaqing, H. Approach to online defect monitoring in fused deposition modeling based on the ariation of the temperature field. *Complexity* **2018**, *2018*, 3426928.
27. Li, Z.; Zhang, D.; Shao, L.; Han, S. Experimental investigation using vibration testing method to optimize feed parameters of color mixing nozzle for fused deposition modeling color 3D printer. *Adv. Mech. Eng.* **2019**, *11*, 1687814019896196. [CrossRef]
28. Li, Y.; Zhao, W.; Li, Q.; Wong, T.; Wang, G. In-situ monitoring and diagnosing for fused filament fabrication process based on vibration sensors. *Sensors* **2019**, *19*, 2589. [CrossRef]
29. Tlegenov, Y.; Feng, L.W.; Soon, H.G. A dynamic model for current-based nozzle condition monitoring in fused deposition modelling. *Prog. Addit. Manuf.* **2019**, *4*, 211–223. [CrossRef]
30. Kim, C.; Espalin, D.; Cuaron, A.; Perez, M.A.; Macdonald, E.; Wicker, R.B. A study to detect a material deposition status infused deposition modeling technology. In Proceedings of the 2015 IEEE International Conference on Advanced Intelligent Mechatronics (AIM), Busan, Korea, 7–11 July 2015; pp. 779–783.
31. Kim, C.; Espalin, D.; Cuaron, A.; Perez, M.A.; Macdonald, E.; Wicker, R.B. Unobtrusive in situ diagnostics of filament-fed material extrusion additive manufacturing. *IEEE Trans. Compon. Packag. Manuf. Technol.* **2018**, *8*, 1469–1476. [CrossRef]
32. Zidek, K.; Maxim, V.; Pitel, J.; Hosovsky, A. Embedded vision equipment of industrial robot for inline detection of product errors by clustering-classification algorithms. *Int. J. Adv. Robot. Syst.* **2016**, *13*, 4901. [CrossRef]
33. Zidek, K.; Pitel, J.; Hosovsky, A. Machine learning algorithms implementation into embedded systems with web application user interface. In Proceedings of the IEEE 21st International Conference on Intelligent Engineering Systems 2017 (INES 2017), Larnaca, Cyprus, 20–23 October 2017; pp. 77–81.

34. Lishchenko, N.; Larshin, V.; Basharov, R. Diagnostics of drilling in numerically controlled machine tools. *Russ. Eng. Res.* **2016**, *36*, 77–80. [CrossRef]
35. Lishchenko, N.; Larshin, V.; Piteľ, J. Detecting systematic and random component of surface roughness signal. *Her. Adv. Inf. Technol.* **2020**, *3*, 61–71.
36. Fastowicz, J.; Bak, D.; Okarma, K. Quality Assessment of 3D Printed Surfaces in Fourier Domain. In Proceedings of the International Conference on Image Processing and Communications, Bydgoszcz, Poland, 13–14 September 2017; pp. 75–81.
37. MacDonald, E.; Burden, E.; Walker, J.; Kelly, J.; Conner, B.; Patterson, C.; Schmidt, A.; Bader, A. Spatial Frequency Analysis for Improved Quality in Big Area Additive Manufacturing (BAAM). In Proceedings of the ASME 2017 International Mechanical Engineering Congress and Exposition, Tampa, FL, USA, 3–9 November 2017; p. 2.
38. Mital', G.; Dobránsky, J.; Ružbarský, J.; Olejárová, Š. Application of laser profilometry to evaluation of the surface of the workpiece machined by abrasive water jet technology. *Appl. Sci.* **2019**, *9*, 2134. [CrossRef]
39. Siklienka, J.Š.M. The effect of a laser beam wavelength on accuracy of surface measurement of unevenness of beechwood by laser beam. *Acta Fac. Xylologiae Zvolen* **2018**, *60*, 137–145.
40. Mitaľ, G. Contactless measurement and evaluation machined surface roughness using laser profilometry. *Transf. Inovácií* **2021**, *43*, 19–24.
41. Kreheľ, R.; Straka, Ľ.; Krenický, T. Diagnostics of production systems operation based on thermal processes evaluation. *Appl. Mech. Mater.* **2013**, *308*, 121–126. [CrossRef]
42. Lednev, V.N.; Sdvizhenskii, P.A.; Asyutin, R.D.; Tretyakov, R.S.; Grishin, M.Y.; Anton, Y.; Stavertiy, A.Y.; Fedorov, A.N.; Pershin, S.M. In situ elemental analysis and failures detection during additive manufacturing process utilizing laser induced breakdown spectroscopy. *Opt. Express* **2019**, *27*, 4612–4628. [CrossRef]
43. Yang, T.; Jin, Y.; Squires, B.; Choi, T.-Y.; Dahotre, N.B.; Neogi, A. In-situ monitoring and ex-situ elasticity mapping of laser induced metal melting pool using ultrasound: Numerical and experimental approaches. *J. Manuf. Processes* **2021**, *71*, 178–186. [CrossRef]
44. Leung, C.L.A.; Marussi, S.; Atwood, R.C.; Towrie, M.; Withers, P.J.; Lee, P.D. In situ X-ray imaging of defect and molten pool dynamics in laser additive manufacturing. *Nat. Commun.* **2018**, *9*, 1355. [CrossRef] [PubMed]
45. Borish, M.; Post, B.K.; Roschli, A.; Chesser, P.C.; Love, L.J.; Gaul, K.T.; Sallas, M.; Tsiamis, N. In-situ thermal imaging for single layer build time alteration in large-scale polymer additive manufacturing. *Procedia Manuf.* **2019**, *34*, 482–488. [CrossRef]
46. Lishchenko, N.; Lazorik, P.; Demčák, J.; Pitel', J.; Židek, K. Quality control monitoring in 3D printing. In *Advances in Design, Simulation and Manufacturing V.*; Springer: Cham, Switzerland, 2022; pp. 31–40.